ORGANOMETALLICS

pubs.acs.org/Organometallics Article

Ligand Reorganization in the Coordination Sphere of a CCC-NHC Pincer Fe Complex and Transient Absorption Spectroscopic Characterization of $[(^{Bu}C^{i}C^{i}C^{Bu})_2Fe]I$

Joshua Mensah, Venkata K. Adiraju, James D. Cope, Robert W. Lamb, Xiao X. Li, Bruno Donnadieu, Igor V. Rubtsov,* Charles Edwin Webster,* and T. Keith Hollis*

Cite This: https://doi.org/10.1021/acs.organomet.3c00386 Read Online

ACCESS | Metrics & More | Article Recommendations | Supporting Information

ABSTRACT: Monoligated and bis-ligated CCC-NHC pincer Fe complexes with *n*-butyl substituents have been synthesized by the Zr metalation/transmetalation route. Both the direct metalation/transmetalation and transmetalation from the isolated $(^{Bu}C^{i}C^{i}C^{Bu})$-$ZrNMe_2Cl_2$, **3,** yielded the octahedrally coordinated Fe(III) bis-ligated complex $[(^{Bu}C^{i}C^{i}C^{Bu})_2Fe]Cl$, **2a**. Transmetalation from *in situ* and isolated $(^{Bu}C^{i}C^{i}C^{Bu})ZrCl_3$, **5**, in the presence of excess TMSCl and 1 equiv of the Fe source yielded the monoligated $(^{Bu}C^{i}C^{i}C^{Bu})FeCl_2$, **4**. Conditions that convert $[(^{Bu}C^{i}C^{i}C^{Bu})_2Fe]^+$, **2**, to $(^{Bu}C^{i}C^{i}C^{Bu})FeCl_2$, **4**, complex have been found. Characterization included ^1H NMR, UV−visible, femtosecond transient absorption spectroscopies, TD-DFT computations, and mass spectroscopy along with X-ray crystallographic structure determinations.

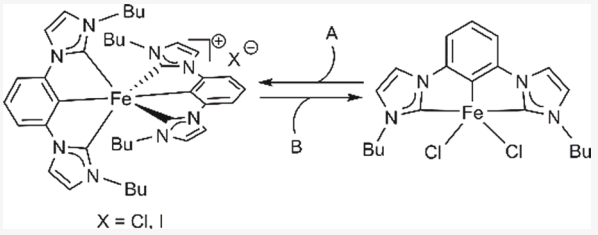

INTRODUCTION

Ligands that chelate metals in a tridentate and primarily meridional geometry "pincer ligands" have recently become ubiquitous in organometallic chemistry.[1,2] The three donors offer multiple sites for electronic and steric tuning of the central metal. Additionally, the terdentate binding mode of pincer ligands enhances the robustness of the corresponding complexes.[2] Many of these complexes have been used in catalytic processes such as cross coupling reactions,[3,4] asymmetric hydrogenation of alkenes,[5] and hydroamination reactions.[6] A pervasive problem in pincer chemistry has been the formation of bis-ligated, octahedrally coordinated, robust complexes (Chart 1A,C,E,F,H,J) which are highly stable and lack open coordination sites.[7,8,17−19,16]

The aforementioned properties of pincer ligands coupled with the strong σ-donation of N-heterocyclic carbenes (NHC) make NHC-based pincers more robust, stable, and relatively nondissociative compared to their phosphine counterparts.[2,20] These properties of NHCs have opened interesting prospects for NHC-based pincer complexes.[21−23] The consensus has been that NHCs are nondissociative ligands;[2,24,25] therefore, incorporating them in the pincer ligand architecture is perceived to make NHC-based pincers even more robust especially when complexed with mid to late first row transition metals.[2,25−29]

Pincer complexes of mid to late first-row transition metals have recently become the subject of much interest due to the natural abundance and nontoxicity of these metals.[5,30−32] Special attention has been given to iron because it is the most abundant metal[32] and the role it plays in the nitrogenase enzyme that catalyzes dinitrogen activation at atmospheric conditions.[32−34] The scarcity of pincer iron complexes is due to the difficulty in controlling the propensity of the ligand to readily rearrange into an octahedral geometry around the metal; especially in the absence of bulky groups.[10,15,18,35,36] Bulky groups such as DIPP, mesitylene, adamantly, and tertbutyl have been used to sterically hinder monoligated complexes rearranging into bis-ligated complexes (Chart 1A → B, C → D, E or F → G, H → I, and J → K)[7,9,35−44,10,45,11−13,15,17−19]; however, the use of these bulky substituents does not always prevent the problem of bis-ligation. In a report by Danopoulos and co-workers, it was established that the introduction of a DIPP groups sometimes did not prevent bis-ligation as the NHC flipped around eliminating the steric hindrance hence enabling the formation of a bis-ligated complex (Chart 1F).[36]

Interestingly, there has been no report of any synthetic route to convert the bis-ligated pincer complexes to the monoligated complexes of these mid to late first-row transition metals.[7,8,47,11−15,36,43,46] Previously, conditions for the synthesis of several CCC-NHC pincer complexes via metalation with $Zr(NMe_2)_4$ followed by transmetalation to other metals such

Received: September 25, 2023
Revised: December 11, 2023
Accepted: December 11, 2023

Chart 1. (A–K) Selected Bis-Ligated Complexes and Bulky Substituents Used in Their Mono-Ligated Complexes

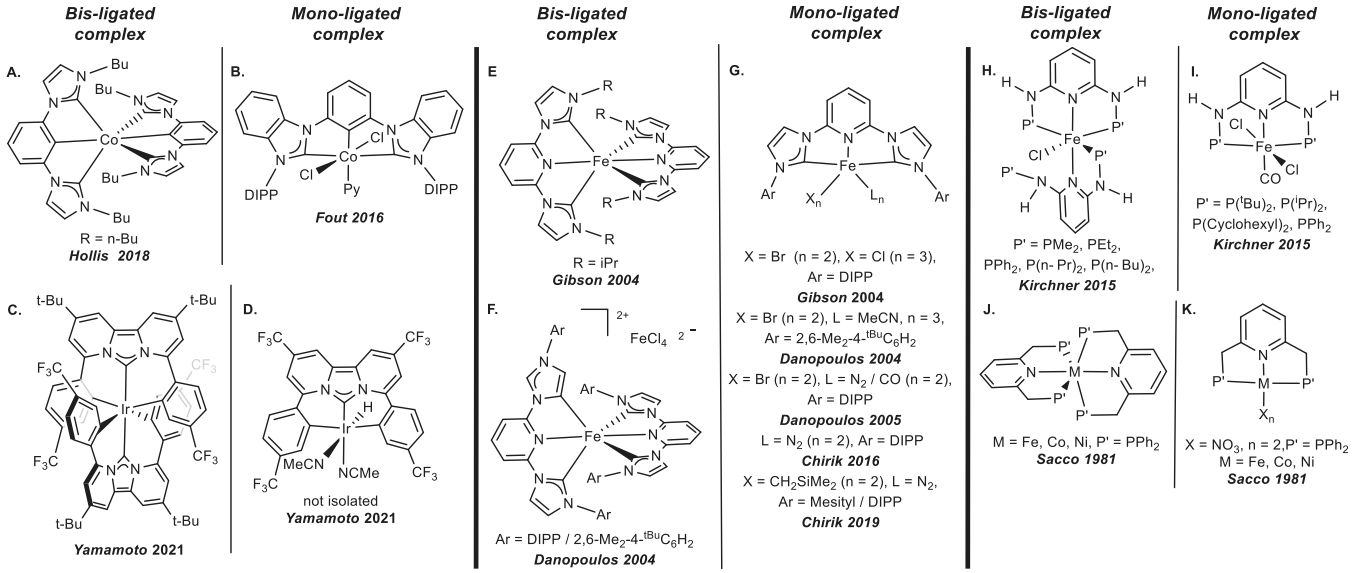

Co, Rh, Pt and Ni have been reported.[43,48−52] A few groups have reported CNC-NHC pincer complexes of iron.[7,36,42,44] Only one group has reported a monoligated CCC-NHC pincer iron complex.[30,53]

In this report, we present the first synthetic route for a monoligated CCC-NHC pincer Fe complex without bulky groups and the synthesis and characterization of the bis-ligated CCC-NHC pincer Fe complexes that were previously included in part in the published patent filed in 2018.[54] Conditions for converting between the monoligated and bis-ligated CCC-NHC pincer Fe complexes are also reported as outlined (Scheme 1).

RESULTS AND DISCUSSION

Synthesis and Characterization. In an attempt to synthesize the pincer iron complex via the *in situ* metalation/transmetalation method, the proligand **1a** was activated using $Zr(NMe_2)_4$. The ^1H NMR spectrum was monitored to ensure the metalation process was complete before the addition of $FeCl_3$ as reported previously for Co, Rh, Pt, and Ni (Scheme 1, **1a** → **2a**).[43,48−52] The ^1H NMR spectrum of the reaction between the white proligand salt and the white crystalline $Zr(NMe_2)_4$ in CD_2Cl_2 was monitored for 1 h until the imidazolium C−H proton signal at 11.3 ppm disappeared and the diastereotopic peaks of the CCC-NHC Zr intermediate appeared at 4.3−4.6 ppm. The yellow solution was reacted with $FeCl_3$ and maintained at room temperature for 8 h (*Route 1a*). The ^1H NMR spectrum became broadened consistent with the formation of a paramagnetic CCC-NHC Fe complex (Scheme 1, **1a** → **2a**). In the ESI-MS of an aliquot of the reaction mixture, a peak with m/z = 698.3539 was observed. When compared with the calculated m/z = 698.3503 for two ligands on one Fe, it established by exact mass and isotope pattern that it was the bis-ligated complex $[(^{Bu}C^iC^iC^{Bu})_2Fe]^+$, **2a** (see SI, Figure S1).[55]

In the ^1H NMR spectrum of complex **2a**, singlet peaks that lacked coupling were observed between 25 and −35 ppm consistent with a paramagnetic Fe center. The peak at −34.42 ppm (2H) was assigned as resonance for the protons para to the Fe center (H_a) because those protons were expected to have the strongest interaction with the Fe center and hence will be the most shifted and the peak at −24.52 ppm (4H) was assigned as resonance for the other phenylene protons ortho to the Fe center (H_b). The observed number of resonances and integrals were consistent with the anticipated (see SI, Figure S2a,b). Room temperature solution magnetic moment of μ_{eff} = 2.32 μ_B consistent with a low spin Fe^{3+} was found for complex

Scheme 1. General Reaction Conditions for Synthesizing the $(^{Bu}C^iC^iC^{Bu})FeCl_2$, 4, and $[(^{Bu}C^iC^iC^{Bu})_2Fe]Cl$, 2a, or $[(^{Bu}C^iC^iC^{Bu})_2Fe]I$, 2b, and Conditions for Converting between 2a or 2b ⟷ 4[a]

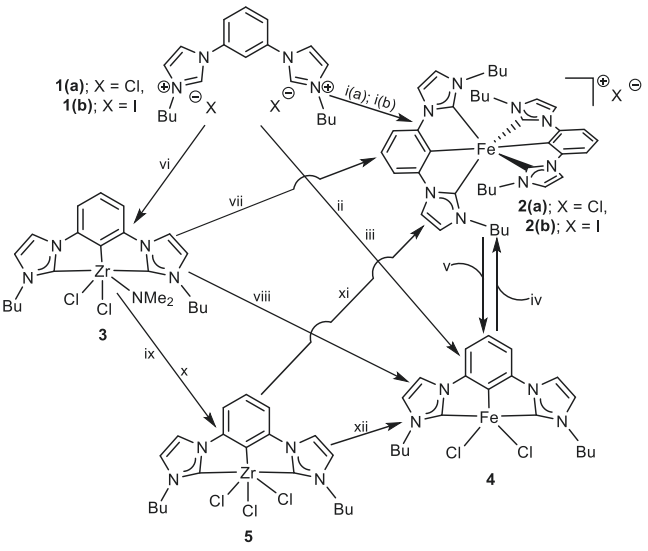

[a](i) (a) $Zr(NMe_2)_4$, DCM, rt, 1 h; (i) (b) FeX_3, 8 h (**1a** → **2a**) and (**1b** → **2b**); (ii) $Zr(NMe_2)_4$, Tol, 160 °C, 16 h (**1a** → **4**); (iii) FeX_3, 8 h (**1a** → **4**); (iv) −TMSCl, FeX_3 (**4** → **2a**); (v) 10 equiv TMSCl, 1.1 equiv $FeCl_3$, THF, 0 °C−rt, 8 h (**2a** → **4**); (vi) $Zr(NMe_2)_4$, Tol, 160 °C, 16 h (**1a** → **3**); (vii) 1.1 equiv FeX_3, DCM, rt, 8 h (**3** → **2a**); (viii) 10 equiv TMSCl, 1.1 equiv FeX_3, DCM, rt, 8 h (**3** → **4**); (ix) TMSCl, DCM, rt, 2 h (**3** → **5**); (x) Tol, 160 °C, 15 min (**3**→**5**); (xi) 1.1 equiv $FeCl_3$, DCM, rt, 8 h (**3** → **5**); (xii) 10 equiv TMSCl, 1.1 equiv FeX_3, DCM, rt, 8 h (**5** → **4**); FeX_3 = $FeCl_3$, $Fe(TMHD)_3$, $Fe(acac)_3$; chemical shorthand: C = atom bound to metal, ^{Bu} − is the substituents, ^{i} − is the imidazolium-based NHC (see ref 55).

https://doi.org/10.1021/acs.organomet.3c00386
Organometallics XXXX, XXX, XXX−XXX

2a.[56] Crystals of complex **2a** suitable for X-ray diffraction were grown via vapor diffusion of hexane into a concentrated DCM solution. An ORTEP representation of complex **2a** is shown in Figure 1. The crystallographic data confirmed two CCC-NHC

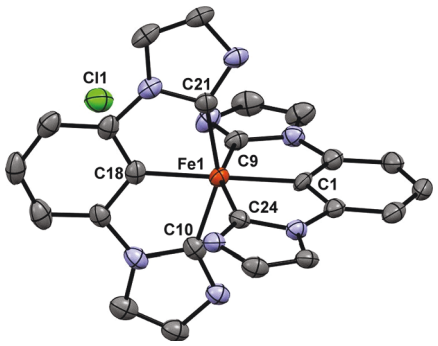

Figure 1. ORTEP representation (50% ellipsoid) of the core molecular structure of $[(^{Bu}C^iC^iC^{Bu})_2Fe]Cl$, **2a**. Hydrogen atoms and butyl chains are omitted for clarity. Selected bond lengths (Å): Fe−C(18), 1.947(6); Fe−C(10), 1.976(6); Fe−C(21), 1.998(6); Fe−C(1), 1.947(6); Fe−C(9), 2.012(6); Fe−C(24), 2.005(6); and angles (deg): C(1)−Fe−C(9) = 77.5(2); C(1)−Fe−C(24) = 77.3(2); C(9)−Fe−C(24) = 154.7(2); C(10)−Fe−C(18) = 78.0(3); C(18)−Fe−C(21) = 76.9(3); C(10)−Fe−C(21) = 154.9(3); C(18)−Fe−C(1) = 179.4(2).

ligands bound to an Fe center in a distorted octahedral coordination sphere with the two ligands oriented perpendicular to each other. A counteranion chloride was observed in the lattice. The closely related structural analogue bis-ligated CNC-NHC Fe of complex **2a** reported had a shorter C^{NHC}−Fe bond distance of 1.952(2) Å compared to the 2.005(6) and 2.012(6) Å observed in complex **2a**. The C^{Phen}−Fe bond length was 1.947(6) Å were slightly longer than N^{Py}−Fe bond lengths of 1.9235(17) Å reported for the CNC-NHC Fe (II). The reported 79.29(8)° and 79.07(8)° N^{Py}−Fe−C^{NHC} bond angles were found to be slightly larger than the C^{Phen}−Fe−C^{NHC} bond angles of 77.3(2)° and 77.5(2)° found in complex **2a**. The N^{Py}−Fe−N^{Py} angle of 177.22° of the CNC-NHC was smaller than the C^{Phen}−Fe−C^{Phen} angle of 179.4(2)° found in complex **2a**.[7] The internal angles were all distorted from the idealized 90° and 180°.[12,15,57] The deviations of the angles from a perfect octahedral can be attributed to the rigid structure of the ligand backbone that constricts the internal angles.[36] The absorption (UV−visible) spectra of complex **2a** were taken in acetonitrile. The solution of complex **2a** had a deep purple color. Two major peaks were observed in the absorption spectra of complex **2a.** The regions of observation of these peaks can be divided into two parts: the ultraviolet (100 nm < λ < 400 nm) and visible (400 nm < λ < 800 nm).[58,59] A broadband between 450 nm < λ < 680 nm which had a λ_{max} at 622 nm (ε = 222 M^{-1} cm^{-1}) that was attributed to d-to-d transitions and a relatively narrower band between 310 nm < λ < 450 nm with a λ_{max} at 352 nm (ε = 2907 M^{-1} cm^{-1}) that was attributed to π-to-π^* transitions were observed for complex **2a** (see SI, Figure S15a).[58] No emission was observable with the naked eye upon irradiation of complex **2a** at 365 or 254 nm. When the samples were irradiated at 410 nm in the fluorimeter, a very weak signal was observed in the visible range with λ_{max} at ∼470 and ∼672 nm (see SI, Figure S15b).

Having established the identity of complex **2a**, other conditions to synthesize the monoligated complex were examined. In an attempt to prevent bis-ligation of the Fe with the CCC-NHC ligand, the less readily displaced TMHD (2,2,6,6-tetramethyl-3,5-heptanedionate) and acac (acetylacetonate) ligands using $Fe(TMHD)_3$ (*Route 1b*) and $Fe(acac)_3$ (*Route 1c*) were investigated as the Fe source (Scheme 1, **1a** → **2a**). Peaks similar to the ones in the ^1H NMR spectrum and ESI-MS of complex **2a** were observed. Due to the poor solubility of the $FeCl_3$ in DCM, the solvent was changed to THF. The proligand salt **1a** and the $Zr(NMe_2)_4$ reacted in THF for 2 h. The $FeCl_3$ was then added to the solution and maintained at room temperature for 8 h. After workup, complex **2a** was isolated as a dark purple powder (69% yield) (Scheme 1, **1a** → **2a**).

In a previous report, it was found that transmetalating from the isolated CCC-NHC-Zr dichloro amido complex often gave different results than the *in situ* metalation/transmetalation reaction route;[43] therefore, the transmetalation from isolated CCC-NHC Zr amido chloride complex, **3**, obtained starting with **1a**,[52] using different Fe sources—$FeCl_3$ (*Route 2a*), $Fe(TMHD)_3$ (*Route 2b*), and $Fe(acac)_3$ (*Route 2c*) were examined. However, in each case. transmetalation using these conditions also yielded complex **2a** (Scheme 1, diagonal **3** → **2a**). The next set of experiment produced a mixture of **2a** and **4** illuminating a pathway that will potentially allow the isolation of pure complex **4**. The coordination sphere of the CCC-NHC-Zr complex **3** was modified *in situ* to generate the trichloride analogue by the addition of TMSCl.[6] After addition of $FeCl_3$ (*Route 1*), the ^1H NMR spectrum was observed to be broadened as typical of paramagnetic species and to be significantly different from that of **2a** (see SI, Figure S4; Scheme 1, **3** → **4**). An aliquot was taken for ESI-MS, and the spectrum contained a new base peak at m/z = 522.0401 that on simulation and comparison of the isotope pattern was found to be consistent with the proposed structural moiety $[C_{20}H_{28}Cl_4FeN_4]$ with one ligand and one Fe center (see SI, Figure S4). The characteristic peak of **2a** at m/z = 698.5 was not observed (see SI, Figure S5). The reaction was then worked up by removing the volatiles to provide a solid. A portion was taken for ESI-MS analysis and the base peak m/z = 698.5 of complex **2a** was observed. Additionally, a new m/z = 412.1 with an isotope pattern that matched the pattern predicted for $[(^{Bu}C^iC^iC^{Bu})FeCl]^+$ that was consistent with the loss of a chloride from complex **4**. Another peak was observed with a m/z = 861.1969 consistent with a chloride bridging two monoligated Fe centers, $[((^{Bu}C^iC^iC^{Bu})ClFe)\text{-}Cl\text{-}(FeCl(^{Bu}C^iC^iC^{Bu}))]^+$,[55] (calcd m/z = 861.1921, Δ = 6.1 ppm) and an isotope pattern that matched the theoretical prediction for the chloro-bridge dimer (see SI, Figure S6). These observations were consistent with the proposed moiety $C_{20}H_{28}Cl_4FeN_4$ (m/z = 522) converting to a mixture of the bis-ligated complex **2a** (major species) and the monoligated species **4** (minor species) during the removal of the volatiles (Scheme 1, **4** → **2a**) (see SI, Figure S5).

These results indicated that the desired monoligated complex **4** was accessible, but conditions for isolation had yet to be identified. Since the trichloride complex $[(^{Bu}C^iC^iC^{Bu})ZrCl_3]$, **5**, seemed to be the best transmetalation agent it was prepared and purified according to the reported procedure for the Ti analogue (see SI, Figure S5).[6] Direct reaction of $[(^{Bu}C^iC^iC^{Bu})ZrCl_3]$, **5**, with $FeCl_3$ (*Route 4*), however, gave a mixture of complex **2a** and complex **4** based

https://doi.org/10.1021/acs.organomet.3c00386
Organometallics XXXX, XXX, XXX−XXX

on the MS observation of peaks with m/z = 698.3579, 412.1190 and 861.1969 corresponding to the bis-ligated and the monoligated species as described above (see SI, Figure S5). Thus, it was hypothesized that in addition to the [($^{Bu}C^{i}C^{i}C^{Bu}$)-$ZrCl_3$], **5**, TMSCl was required for efficient production of complex **4**. The reaction of the isolated [($^{Bu}C^{i}C^{i}C^{Bu}$)$ZrCl_3$], **5**, 10 equiv TMSCl, 1 equiv of $FeCl_3$ (*Route 1a*) and stirring for 8 h in DCM yielded a thick red paste (Scheme 2). DCM was

Scheme 2. Best Synthesis of ($^{Bu}C^{i}C^{i}C^{Bu}$)$FeCl_2$, 4

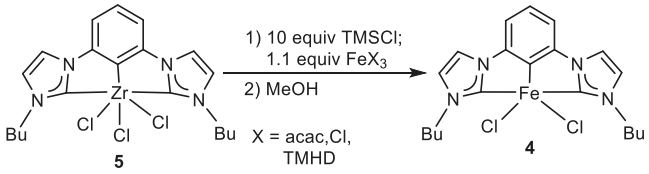

added to the paste, and it was filtered through celite. The volatiles were removed producing a dark red sticky concentrate. An aliquot of this sticky concentrate was analyzed by ESI-MS. The peaks observed at the m/z = 412 [($^{Bu}C^{i}C^{i}C^{Bu}$)FeCl]$^+$ and the m/z = 861 [(($^{Bu}C^{i}C^{i}C^{Bu}$)ClFe)-Cl-(FeCl($^{Bu}C^{i}C^{i}C^{Bu}$))]$^+$[55] were consistent with complex **4** (see SI, Figure S7). The characteristic m/z = 698 peak of the bis-ligated complex **2a** was *not* observed. Upon addition of MeOH, complex **4** precipitated out of the sticky concentrate and was isolated as a bright red-orange powder 77% yield. Analogous transmetalation reactions using Fe(TMHD)$_3$ (*Route 1b*) yielded 60% and when Fe(acac)$_3$ (*Route 1c*) yielded 37% of complex **4** (Scheme 2). The absence of either a "TMHD" and "acac" in the crystal structure was likely due to the silylation of these two species by the TMSCl.

A combination of ^{1}H NMR, solution magnetic moment measurement (Evans method), elemental analysis, ESI-MS, UV−visible, and XRD spectroscopies were used to complete the characterization. In the ^{1}H NMR spectrum, broadened peaks due to lack of coupling which was characteristic of a paramagnetic Fe center were observed between 33.56 ppm and −27.64 ppm (see SI, Figure S8). The peak at 33.56 ppm was assigned as the protons para to the Fe center because those protons were expected to have the strongest interaction with the Fe center and hence will be the most shifted and the peak at −27.64 ppm was assigned as the other phenylene protons ortho to each NHC ring. Magnetic moment of μ_{eff} = 5.7 consistent with a high spin Fe^{3+} was found for complex **4**.[56] In the absorption spectra of complex **4**, a relatively sharp band around 320 nm < λ < 400 nm with a λ_{max} at 360 nm (ε = 1368 M^{-1} cm^{-1}) which was attributed to π-to-π^* transitions was observed (see SI, Figure S17a).[58] No emission was observable with the naked eye upon irradiation of complex **4** at 365 or 254 nm. When the samples were irradiated at 350 nm in the fluorimeter, a very weak signal was observed in the visible range with λ_{max} at ∼ 390 and ∼ 640 nm (see SI, Figure S17b).

Crystals suitable for X-ray diffraction were grown via vapor diffusion of hexane into a saturated DCM solution. The X-ray crystallographic data were consistent with complex **4** (Figure 2). The NHC donor carbenes occupied positions trans to each other and the two chlorides were directed out of the plane of the CCC-NHC ligand moiety. The butyl chains were oriented trans to each other giving the complex a C_{2V} symmetry. The geometry index (τ_5) around the CCC-NHC Fe was calculated as 0.99 which is consistent with a trigonal bipyramidal

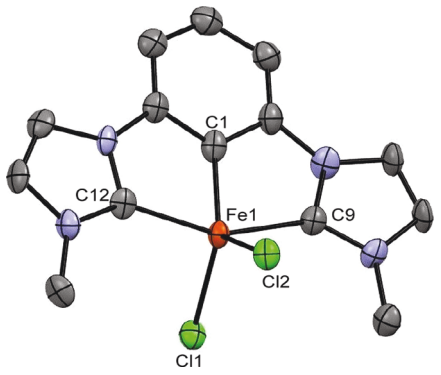

Figure 2. ORTEP representation (50% ellipsoid) of the core molecular structure of ($^{Bu}C^{i}C^{i}C^{Bu}$)$FeCl_2$, **4**. Hydrogen atoms are omitted, and butyl chains truncated for clarity. Bond lenghts (Å): Fe(1)−C(1) 1.96(1), Fe(1)−C(9) 2.04(1), Fe(1)−C(12) 2.03(1), Fe(1)−Cl(1) 2.276(4), Fe(1)−Cl(2) 2.311(3) and angles (deg): C(1)−Fe(1)−C(9) 75.3(5), C(1)−Fe(1)−C(12) 76.9(5), C(9)−Fe(1)−C(12) 152.1(5), C(1)−Fe(1)−Cl(1) 138.0(3), C(1)−Fe(1)−Cl(2) 119.6(3), Cl(1)−Fe(1)−Cl(2) 110.3(1).

coordination around the Fe center.[60] The Cl−Fe−Cl bond angle was 110.3°. The metric data of complex **4** was compared to the other octahedrally coordinated CCC-NHC Fe(III) complex reported.[30] The C^{Phen}−Fe bond length in complex **4** was found to be 1.960(1) Å compared to the reported 1.920(6) Å. The C^{NHC}−Fe bonds in complex **4** were 2.04(1) and 2.03 (1) Å compared to 1.999(7) and 1.994(7) Å reported. The Fe−Cl bonds in complex **4** were 2.311(3) and 2.276(4) Å compared to the 2.363(2) and 2.259(2) Å reported. The C^{NHC}−Fe−C^{NHC} bond angle in complex, **4**, was found to be 152.1(5)° which was slightly smaller compared to the reported 158.3(3)°. The C^{NHC}−Fe−C^{Phen} bond angles in complex, **4**, 75.3(5)° and 76.9(5)°, were found to be slightly smaller compared to the 79.8(3)° and 79.3(3)° in the previously reported structure.[30]

As illustrated in Scheme 1 (**4** → **2a**), the monoligated complex **4** will undergo ligand exchange to generate bis-ligated complex **2a**. The possibility of reversing this process was investigated (Scheme 3). First, treatment of bis-ligated

Scheme 3. Synthesis of ($^{Bu}C^{i}C^{i}C^{Bu}$)$FeCl_2$, 4

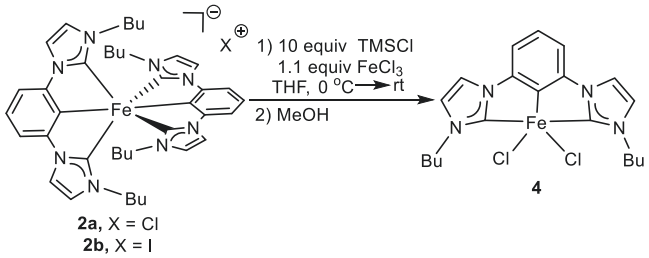

complexes (**2a** or **2b**) with another equivalent of $FeCl_3$ alone did not reverse the process. As TMSCl was required in the successful synthesis of complex **4**, treatment of bis-ligated complexes with $FeCl_3$ and TMSCl was evaluated. Thus, a THF solution of the bis-ligated complexes (**2a** or **2b**) was cooled to 0 °C, excess TMSCl was added dropwise, and after warming to room temperature, $FeCl_3$ (1 equiv) was added. The reaction was monitored by MS for disappearance of the m/z = 698 peak [M−X]$^+$ (where X = Cl or I) of the starting material complexes **2a** or **2b**. The mysterious m/z = 522 peak appeared again;

https://doi.org/10.1021/acs.organomet.3c00386
Organometallics XXXX, XXX, XXX−XXX

however, all efforts to isolate, crystallize, or further characterize the m/z = 522 species provided no further insight. The process was repeated at scale, and the volatiles were removed. Upon addition of MeOH a bright red-orange powder precipitated. The ^{1}H NMR spectrum and mass spectra of the isolated powder were consistent with the previously isolated (^{Bu}C^{i}C^{i}C^{Bu})FeCl$_2$ (Scheme 3). Thus, an efficient method for decomplexing the bis-ligated complex, **4**, was obtained.

It is appropriate to comment that at present, the exact function of the TMSCl as the effective reagent for decomplexing is not fully understood or experimentally elaborated. However, two facts regarding NHC-TMS (NHC-SiMe$_3$) adducts are well-established in the literature. First, metal NHC complexes will react with TMSCl to produce the NHC-TMS adduct.[64] Further, the NHC-TMS adducts have been used as carbene transfer reagent to metals such as Ce, Y, Pd, Ni, and Au.[61−63] The utilization of these two pieces of information was demonstrated in a report by Turner and co-workers. In their study, they applied TMSCl to break a bond between a metal and a NHC creating the NHC-TMS species. This bond was subsequently employed to transfer the NHC to the metal once the TMS group was eliminated.[64] Based on these reports, we hypothesize that the NHC-TMS adduct is first formed by partial decomplexation, then with FeCl$_3$ present the ligand is transferred.[61−63] As the MS were collected in acetonitrile under ambient (wet solvents, humid conditions), the TMS groups were cleaved from the partially bound ligand leading to the observation of the m/z = 522 in the ESI-MS (see SI, Figures S10 and S11).[64] Upon working up the reaction by the addition of MeOH, the TMS group is cleaved from the NHC-TMS species by forming the strong Si−O bond, producing the monoligated compound **4**. It has been previously reported that the NHC-TMS bonds undergo facile, essentially immediate, hydrolysis in the presence of water supporting the MS observations herein.[65] A similar observation was reported for the reactivity of NHC-TMS species with MeOH that is expected to produce TMSOMe as the other product.[64]

Transient Absorption Studies. Development of transition metal complexes as photosensitizers in photocatalytic applications[66] has been ongoing for several years. The most commonly used metal for such applications is ruthenium[67,68] because of the long charge transfer state lifetimes that occur from the large orbital splitting for second and third row metals.[69] However, more earth-abundant metals such as iron are desired due to their low cost and lower toxicity. Though there are several investigations into this,[18,70−72] there is still a challenge[73] to obtain complexes with excited state (ES) lifetimes longer than a few tens of picoseconds (ps).[74] Recently, it has been shown that one of the most promising ways to achieve longer ES lifetimes is by increasing the number of N-heterocyclic carbene (NHC) ligands coordinated to a metal center;[70,75] however, solubility in organic solvents becomes an issue when dealing with multiply charged complexes. Excited-state dynamics of complex **2b** was studied using transient absorption spectroscopy featuring instrument response function of 150 fs.[76] The sample was excited at 400 nm and probed in a wide range of wavelengths ranging from 450 to 1050 nm. The transient spectra feature a broad excited-state absorption band with the maximum at about 500 nm. The transient spectrum changes little with the delay time between the pump and probe, suggesting that a single excited state is formed upon excitation (Figure 3a,b). Transient

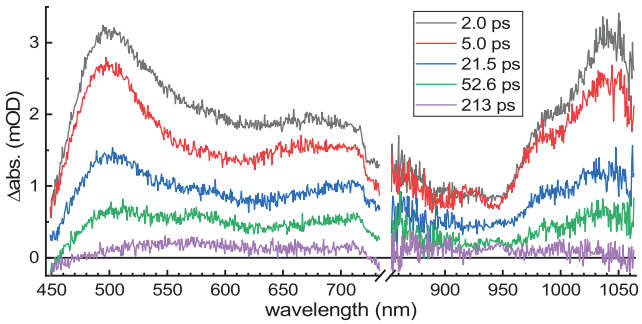

3a

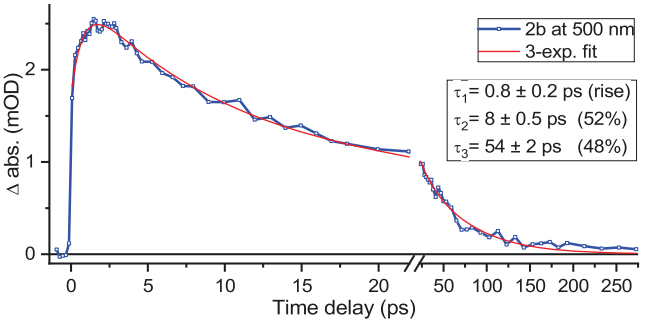

3b

Figure 3. (a) Transient absorption spectrum of **2b** at time delays indicated as the inset. (b) Transient kinetics of **2b** at 500 nm integrated within ± 2 nm window. The characteristic times are shown as the inset. The amplitudes of the decay components are given in parentheses.

kinetics recorded at ca. 500 nm can be well fitted with a three-exponential function with characteristic times of 0.8, 8, and 54 ps. The fast component of 0.8 ps is associated with a rise of transient absorption across the spectrum and is likely due to vibronic relaxation of the excited state. The two decay components, 8 and 54 ps, feature similar amplitudes (Figure 3b, inset). Because the two components are associated with similar transient spectra, they can be assigned to different conformations of **2b**. The mean lifetime of 30.1 ps was obtained.

TD-DFT computations were also performed to simulate these spectra and attain a greater understanding of the excitations involved. The feature present at ∼ 410 nm in the simulated GS absorption spectrum (Figure 4) arises from two separate transitions. The 419 nm transition corresponds to an excitation of a ß electron, with an expectation value reflective of a quartet state (S^2 = 2.753) The 403 nm transition corresponds to an excitation of an α electron with an expectation value reflective of a doublet state (S^2 = 0.871). Both transitions have a similar oscillator strength and are near to the pump wavelength of 400 nm used prior to measurement of the transient absorption spectra. Because the ES kinetics indicate that only a single species is present, we believe that population of the doublet state is more likely. Thus, to obtain the ES geometry, TD-DFT optimizations were carried out with the 403 nm transition selected as target state. Before simulating the transient absorption spectrum for the optimized ES geometry, the best approximation of the ES wave function is needed. Inspection of the target transition at the optimized ES geometry showed that it is predominantly a result of a single α

https://doi.org/10.1021/acs.organomet.3c00386
Organometallics XXXX, XXX, XXX−XXX

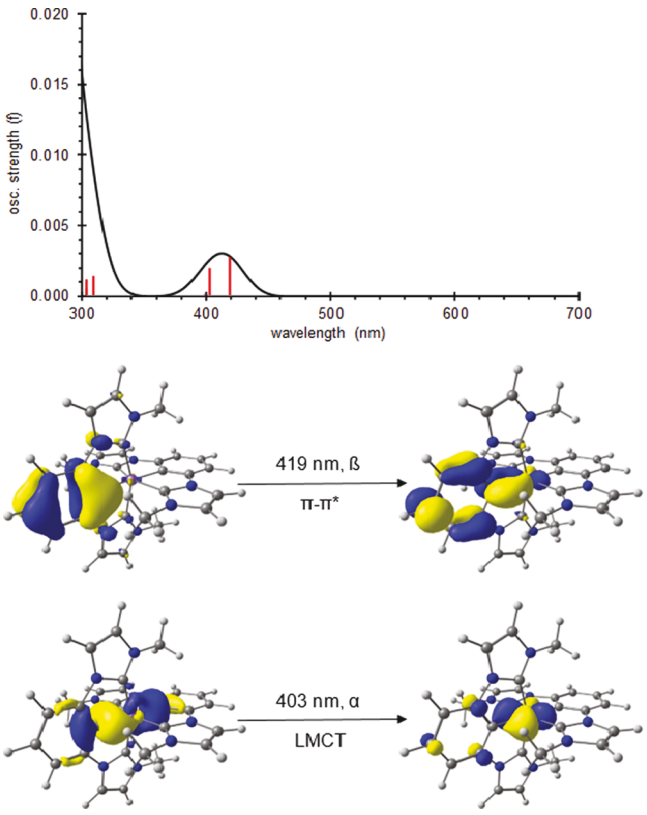

Figure 4. Simulated ground state absorption spectrum and NTOs.

excitation. Performing a swap of these two orbitals provides a reference wave function that is analogous to the result of that α excitation. A TD-DFT single-point computation on this new reference wave function produced the spectrum shown in Figure 5. Indeed, the features present in this spectrum are highly reminiscent of the experimental transient absorption spectrum (see SI, Figure S16). The natural transition orbitals (NTOs) in Figure 5 demonstrate that the ~600 nm band appears to be from a combination of an Fe d−d and a LLCT excitation. Meanwhile, the ~440 nm band is due to a $\pi-\pi^*$ excitation in one of the phenyl rings (Figure 5) which also results in some back-bonding character to the Fe center.

CONCLUSIONS

A route for synthesizing air and moisture-stable CCC-NHC bis and monoligated Pincer Fe complexes $[(^{Bu}C^iC^iC^{Bu})_2Fe]Cl$, **2a**, and $(^{Bu}C^iC^iC^{Bu})FeCl_2$, **4**, taking advantage of the $Zr(NMe_2)_4$ metalation/trans metalation approach has been developed. In situ metalation/ transmetalation yielded complex **2a**. Transmetalation from isolated complex Zr amido complex **3** yielded **2a**. A combination of TMSCl, Zr amido complex **3** and an iron source produced an intermediate which on removing volatiles yielded a mixture of **2a** and **4**. Transmetalating from isolated complex **5** only also yielded a mixture of **2a** and **4**. TMSCl, complex **5** and an iron source, yielded **4** that was isolated in good yield. The intermediate with m/z = 522 has so far eluded further structural characterization. A new method for converting $[(^{Bu}C^iC^iC^{Bu})_2Fe]Cl$, **2a**, or $[(^{Bu}C^iC^iC^{Bu})_2Fe]I$, **2b**, back to $(^{Bu}C^iC^iC^{Bu})FeCl_2$, **4**, has been reported. This method may open a path for the decomplexation of other bis-ligated tridentate metal complexes.

The UV-pump/Vis-probe spectra show that the excited states decay nearly concomitantly at all wavelengths while

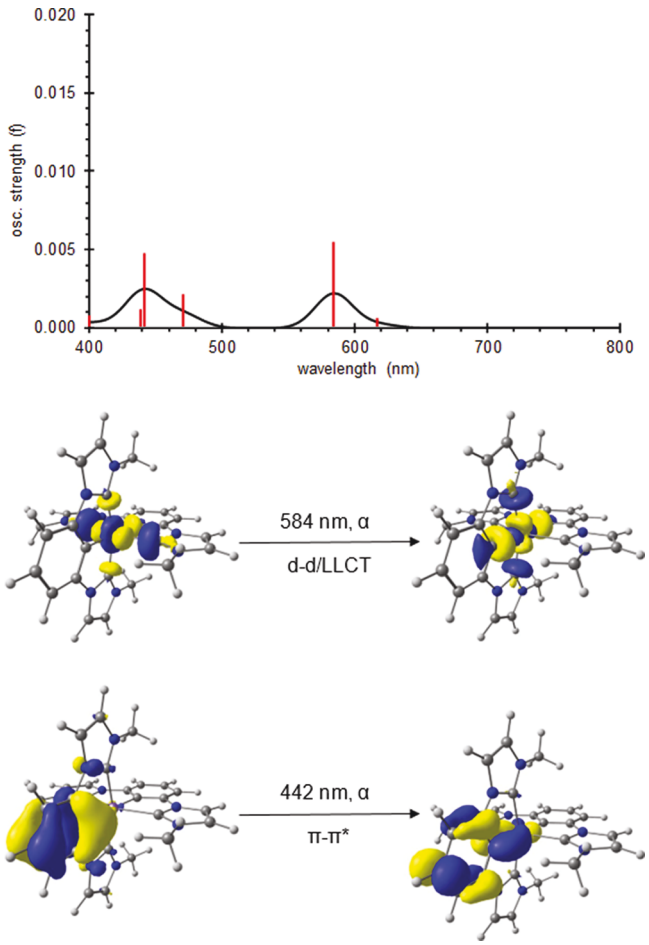

Figure 5. Simulated excited state transient absorption spectrum and NTOs.

featuring two decay constants (8 and 54 ps) with almost the same amplitudes. The mean lifetime of the excited state is ca. 30 ps, offering a promise. The simulated spectra from TD-DFT computations cleanly reproduce both the GS absorption and ES transient absorption of **2b** and offer insight into the nature of the long-lived ES and its transient absorption spectrum.

EXPERIMENTAL DETAILS

General Details. Reagents and starting materials were purchased from commercial sources and used without further purification. All experiments were conducted under nitrogen unless otherwise noted. The proligand imidazolium salts ($[(^{Bu}C^iC^iC^{Bu})H_3]^{2+}Cl_2$) **1a** and ($(^{Bu}C^iC^iC^{Bu})Zr(NMe_2)Cl_2$) **3** were prepared according to previously reported literature procedures.[52,77] The $(^{Bu}C^iC^iC^{Bu})ZrCl_3$ **5** was synthesized according to previously reported procedure for the Ti analogue.[6] The ^{1}H NMR spectra were referenced against the residual solvent peak in DMSO-D_6, $CDCl_3$, CD_2Cl_2, or CD_3CN. Elemental analyses were carried out on a Unicube Elementar. The UV−visible spectra were collected on a Shimadzu UV-2600i spectrophotometer. A suitable single-crystal was selected and analyzed on a Bruker APEX-II CCD diffractometer. The crystal was kept at 100 K during data collection. Using Olex2, the structure was solved with the ShelXT structure solution program using direct methods and refined with the ShelXL refinement package using least-squares minimization. Nanosecond transient absorption data in the UV and visible spectral regions were recorded with an LKS 60 spectrometer (Applied Photophysics) using a Nd3+:YAG laser (Brilliant, Quantel) equipped with second and third harmonic generation units and an optical parametric oscillator (OPOTEK, 420−670 nm) for tunable excitation.

https://doi.org/10.1021/acs.organomet.3c00386
Organometallics XXXX, XXX, XXX−XXX

Transient absorption spectra were constructed from transient decays collected at 10 ns intervals following pulsed laser excitation. The excitation wavelength used for these complexes was 400 nm. Samples were bubbled with N_2(g) for 20 min prior to the measurements.

Computational Methods. All computations were carried out using Revision C.01 of the Gaussian 16[78] suite of programs with default (10−8) SCF convergence criteria. The LC-ωhPBE[79] method was used for all computations with the PCM implicit solvation model using parameters consistent with acetonitrile as the solvent. The basis set and ECP combination used throughout employed the def2-TZVP[80] basis set and ECP for the Fe center and the def2-SV(P)[80] basis and ECP for all other atoms. The Fe complex was optimized with a doublet wave function in D_2d symmetry and confirmed to be a minimum by an analytical frequency computation at the same level of theory resulting in 0 imaginary modes. To simulate spectra, the first 50 vertical excitation energies solved iteratively [TD(ROOT = 1,NSTATES = 50)] using TD-DFT single-point computation at the same level of theory. Excited state geometries were obtained from TD-DFT optimizations, again solving the first 50 vertical excitation energies. NTOs of the relevant transition densities were rendered using Chemcraft.[81]

*Synthetic Details Synthesis of Bis[1,3-bis(n-butyl-imidazol-2′-ylidene) phenylene) iron (III)] Chloride, [(^{Bu}C^{i}C^{i}C^{Bu})$_2$Fe]Cl, **2a**. Route 1a.* Salt **1a** (0.0795 g, 0.200 mmol), $Zr(NMe_2)_4$ (0.0697g, 0.260 mmol), and THF (15.0 mL) were combined under an inert atmosphere yielding a clear golden solution. After 2 h, $FeCl_3$ (41.3 mg, 0.250 mmol) and stirred for about 10 min producing a clear purple solution. The purple solution was left to stir overnight yielding an opaque black solution. Water (40 μL, 2.2 mmol) was added, producing a white precipitate. The black supernatant was filtered, and the volatiles were removed. The solid was then washed with hexanes (3 × 2 mL). Volatiles were removed followed by dissolving in 5 mL DCM andADDINg 5 mL water and shaken vigorously and left to settle. The colorless aqueous layer became red, and the organic layer became a dark purple. The organic layer was separated, and the volatiles were removed yielding a dark purple powder (51.0 mg, 69.2%). X-ray quality crystals were grown by vapor diffusion with hexane and DCM. Anal. calcd for $C_{40}H_{50}ClFeN_8$•0.45 CH_2Cl_2; C, 62.90; H, 6.64; N, 14.51; found C, 62.74; H, 6.87; N, 14.85. ^{1}H NMR (500 MHz, $CDCl_3$): δ 24.50, 9.17, 1.93, 0.95, −0.97, −2.62, −34.43 ppm. μ_{eff} = 2.32 μ_B. HRMS (ESI-TOF) calcd for $C_{40}H_{50}FeN_8$ $[M-Cl]^+$ = 698.3503, obs m/z = 698.3539.

Route 1b. Salt **1a** (0.0140 g, 0.0234 mmol) and $Zr(NMe_2)_4$ (0.0960 g, 0.359 mmol) were combined in CD_2Cl_2 under an inert atmosphere yielding a clear golden solution. After 2 h, $Fe(TMHD)_3$ (0.00120 g, 0.0184 mmol) was added and stirred for about 10 min producing a clear purple solution. The purple solution was left to stir overnight yielding an opaque black solution. An aliquot gave ESI and ^{1}H NMR spectra as observed in *route 1a* (see SI, Figures S1 and S2).

Route 1c. Salt **1a** (0.0156 g, 0.0394 mmol) and $Zr(NMe_2)_4$ (0.0106 g, 0.0397 mmol) were combined in CD_2Cl_2 under an inert atmosphere yielding a clear golden solution. After 2 h, $Fe(acac)_3$ (0.0065 g, 0.0184 mmol) was added and stirred for about 10 min producing a clear purple solution. The purple solution was left to stir overnight yielding an opaque black solution. Analysis of an aliquot gave ESI and ^{1}H NMR spectra as observed in *route 1a* (see SI, Figures S1 and S2).

Route 2a. Complex **3** ((^{Bu}C^{i}C^{i}C^{Bu})$ZrCl_2NMe_2$) (0.0134 mg, 0.250 mmol) and $FeCl_3$ (0.0064 g, 0.039 mmol) were combined in DCM under an inert atmosphere and stirred for 8 h yielding an opaque black mixture. Water (40 μL, 2.2 mmol) was added, producing a white precipitate. The black supernatant was filtered through celite, and the volatiles were removed. The solid was then washed with hexanes (2 × 0.5 mL). Volatiles were removed followed by dissolving in 5 mL DCM and adding 5 mL water and shaken vigorously and leaving to settle. The colorless aqueous layer became red, and the organic layer became a dark purple. The organic layer was separated, and the volatiles were removed yielding a dark purple powder (5.3 mg, 57.8%) ^{1}H NMR (500 MHz, CD_3CN): δ 24.50, 9.17, 1.93, 0.95, −0.97, −2.62, −34.43 ppm. HRMS (ESI-TOF) calcd for $C_{40}H_{50}FeN_8$ $[M-Cl]^+$ = 698.3503, obs m/z = 698.3539 (see SI, Figures S1 and S2).

Route 2b. ((^{Bu}C^{i}C^{i}C^{Bu})$ZrCl_2NMe_2$) (10.6 mg, 0.0201 mmol) and $Fe(acac)_3$ (8.80 mg, 0.025 mmol) were combined in CD_2Cl_2 under an inert atmosphere yielding and stirred for 2 h producing a clear purple solution. An aliquot gave ESI and ^{1}H NMR spectra as observed in *route 2a* (see SI, Figures S1 and S2).

Route 2c. ((^{Bu}C^{i}C^{i}C^{Bu})$ZrCl_2NMe_2$) (11.3 mg, 0.021 mmol) and $Fe(TMHD)_3$ (17.6 mg, 0.029 mmol) were combined in CD_2Cl_2 under an inert atmosphere yielding and stirred for 2 h producing a clear purple solution. An aliquot gave ESI-MS and ^{1}H NMR spectra as observed in *route 2a* (see SI, Figures S1 and S2).

*Synthesis of Bis(1,3-bis(n-butyl-imidazol-2′-ylidene) phenylene) iron(III)] Iodide, [(^{Bu}C^{i}C^{i}C^{Bu})$_2$Fe]I, **2b**. Route 1a.* 1,3-bis(1-butylimidizol-3-yl) benzene diiodide, **1b** (0.1154 g, 0.20 mmol) and $Zr(NMe_2)_4$ (0.0724 g, 0.27 mmol) were combined in THF (15 mL) under an inert atmosphere and stirred for 2 h. $FeCl_3$ (0.046 g, 0.28 mmol) was added and stirred overnight. Water (40 μL, 2.2 mmol) was added, producing a precipitate that was removed and washed with MeCN (3 × 5 mL) and concentrated and dried under vacuum. The product was isolated via silica column chromatography. DCM was used to remove impurities, then MeCN to collect a dark blue band which was concentrated giving the product as a dark blue glassy solid (0.0504 g, 61.2%). X-ray quality crystals were obtained by vapor diffusion of hexane with a CH_2Cl_2 solution. Anal. calcd for $C_{40}H_{50}FeN_8I$; C, 58.19; H, 6.10; N, 13.57; O, 3.15; found C, 58.40; H, 5.79; N, 11.61. ^{1}H NMR (CD_2Cl_2, 500 MHz): δ 24.66 (s, 4H), 9.21 (s, 8H), 1.90 (s, 12H), 0.95 (s, 12H), −0.98 (s, 8H), −2.55 (s, 4H), −36.52 (s, 2H). HRMS (ESI-TOF) calcd for $C_{40}H_{50}FeN_8$ $[M-I]^+$ = 698.3503, obs m/z = 698.3486 (see SI, Figures S1 and S2).

Route 1b. Salt **1b**, 3-bis(1-butylimidizol-3-yl)benzene diiodide, **1b** (0.0961 g, 0.1671 mmol) and $Zr(NMe_2)_4$ (0.0614 g, 0.2390 mmol) were combined in THF (15 mL) under an inert atmosphere and stirred for 2 h. $FeCl_2$ (0.046 g, 0.28 mmol) was added and stirred overnight. Water (40 μL, 2.2 mmol) was added, producing a precipitate that was removed and washed with MeCN (3 × 5 mL) and concentrated and dried under vacuum. The product was isolated via silica column chromatography. DCM was used to remove impurities, then MeCN to collect a dark blue band which was concentrated giving the product as a dark blue glassy solid (0.0344 g, 50.2%).

*Synthesis of a Mixture of [(Bis-1,3-bis(n-butyl-imidazol-2′-ylidene) phenylene) iron (III)] Chloride, [(^{Bu}C^{i}C^{i}C^{Bu})$_2$Fe]Cl, **2a** and [1,3-Bis (n-butyl-imidazol-2-ylidene phenylene iron (III) dichloride] [(^{Bu}C^{i}C^{i}C^{Bu})$FeCl_2$], **4**. Route 1a.* Complex **3** ((^{Bu}C^{i}C^{i}C^{Bu})$ZrCl_2NMe_2$) (30.6 mg, 0.06 mmol), $FeCl_3$ (12.4 mg, 0.077 mmol), TMSCl (100 μL, 0.790 mmol), and DCM were combined under an inert atmosphere and stirred for 8 h yielding a pale red mixture after 8 h. In a HRMS (ESI-TOF) of crude reaction calcd for $C_{20}H_{28}Cl_4FeN_4$ $[M]^+$ = 522.0385, obs m/z = 522.0401 was observed (see SI, Figure S4). The reaction mixture was filtered through celite and the volatiles were removed yielding a brown powder. HRMS (ESI-TOF) calcd for $C_{40}H_{50}FeN_8$ $[M-Cl]^+$ = 698.3503, obs m/z = 698.3506, calcd for $C_{20}H_{25}FeN_4Cl$ $[M-Cl]^+$ = 412.1112, obs m/z = 412.1124, calcd for $C_{40}H_{50}Cl_3Fe_2N_8$ $[2M-Cl]^+$ = 859.1921, obs m/z = 859.1955.

Route 2. Complex **5** ((^{Bu}C^{i}C^{i}C^{Bu})$ZrCl_3$) (22.6 g, 0.044 mmol), $FeCl_3$ (9.09 mg, 0.0561 mmol), and DCM were combined under an inert atmosphere and stirred for 8 h yielding a pale red mixture. In a HRMS (ESI-TOF) of crude reaction calcd for $C_{20}H_{28}Cl_4FeN_4$ $[M]^+$ = 522.0385, obs m/z = 522.0401 was observed (see SI, Figure S5). The reaction mixture was then filtered through celite. Volatiles were removed yielding a brown powder. ESI-MS shows a mixture of complex **2** and complex **4**. HRMS (ESI-TOF) calcd for $C_{40}H_{50}FeN_8$ $[M-Cl]^+$ = 698.3503, obs m/z = 698.3506, calcd for $C_{20}H_{25}FeN_4Cl$ $[M-Cl]^+$ = 412.1112, obs m/z = 412.1124, calcd for $C_{40}H_{50}Cl_3Fe_2N_8$ $[2M-Cl]^+$ = 859.1921, obs m/z = 859.1955.

*Synthesis of [1,3-Bis(n-butyl-imidazol-2-ylidene) phenylene trichloro zirconium (IV)] [(^{Bu}C^{i}C^{i}C^{Bu})$ZrCl_3$], **5**.* Under an inert atmosphere, complex **3** (255 mg, 0.484 mmol), TMSCI (0.600 mL, 4.74 mmol), and dichloromethane (25.0 mL) were combined in a

https://doi.org/10.1021/acs.organomet.3c00386
Organometallics XXXX, XXX, XXX−XXX

flask. The resulting mixture was stirred at room temperature for 2 h. Volatiles were removed under reduced pressure to obtain white solid. Toluene (25.0 mL) was added to the residue and the resulting mixture was heated for 15 min at 160 °C. The mixture was cooled to room temperature during which white solid precipitated. The solids were dried in a vacuo to give **5** as a colorless crystal (180 mg, 74.2%): ^{1}H NMR spectrum (300 MHz, CD_2Cl_2) δ 8 7.51 (d, J = 1.9 Hz, 2H), 7.35 (dd, J, = 8.3 Hz, J = 7.3 Hz, 1H), 7.16 (s, 1H), 7.13 (s, 1H), 7.11 (d, J = 1.9 Hz, 2H), 4.42 (t, J = 7.4 Hz, 4H), 2.03 (q, J = 7.5 Hz, 4H), 1.49 (s, J = 7.4 Hz, 4H), 1.01 (t, J = 7.4 Hz, 6H). Anal. calcd for $C_{20}H_{25}Cl_3N_4Zr{\bullet}H_2O$: C, 44.73; H, 5.07; N, 10.43; found C, 44.43; H, 4.71; N, 10.50.

*Synthesis of [1,3-Bis (n-butyl-imidazol-2-ylidene phenylene iron (III) dichloride] [($^{Bu}C^iC^iC^{Bu}$)$FeCl_2$], **4**. Route 1a.* $FeCl_3$ (36.3 mg, 0.220 mmol) was suspended in DCM (6 mL) in a flask. Separately, compound **5** (86.0 mg, 0.170 mmol), TMSCl (120 μL, 0.950 mmol), and DCM (6 mL) were added and stirred for 5 min. The content of the latter was added to the $FeCl_3$/DCM suspension. The resulting mixture was left to stir for 8 h yielding a red paste. DCM (200 mL × 2) was added to the paste, shaken vigorously, and allowed to settle. The supernatant was filtered through celite followed by concentrating to dryness. The concentrate was then dissolved in minimum DCM and then hexanes added to precipitate out the product. The product was collected over frit and then dried. MeOH was added to the brick red powder to precipitating out a bright red-orange powder which was collected over frit and dried (57.5 mg, 77.18%). Single crystals for XRD were grown via vapor diffusion with DCM and hexanes. Anal. calcd for $C_{20}H_{25}Cl_2N_4Fe$: C, 53.60; H, 5.62; N, 12.50; found C, 53.58; H, 5.64; N, 12.57. ^{1}H NMR (500 MHz, DMSO-D_6): δ 33.56, 7.89, 3.39, 1.97, −1.55, −4.08, −27.64. μ_{eff} = 5.7 μ_B. HRMS (ESI-TOF) calcd for $C_{20}H_{25}FeN_4Cl$ $[M-Cl]^+$ = 412.1112, obs m/z = 412.1192, calcd for $C_{40}H_{50}Cl_3Fe_2N_8$ $[2M-Cl]^+$ = 859.1921, obs m/z = 859.1969.

Route 1b. Complex **5** (0.0119 g, 0.0230 mmol) was dissolved in CD_2Cl_2 and TMSCl (60 μL, 0.474 mmol) was added dropwise to the CD_2Cl_2-**5** solution. $Fe(TMHD)_3$ (0.0138 g, 0.0230 mmol) was added to the content of the NMR tube and sonicated for 15 min. The resulting solution was left to stir for 8 h and then filtered through celite. The red filtrate was concentrated down and layered with hexanes and left in a freezer at −35 °C freezer overnight. Red crystals (6.20 mg, 60.3%) were collected for XRD measurement. An aliquot gave ESI and ^{1}H NMR spectra as observed in route 1 above (see SI, Figures S7 and S8).

Route 1c. Complex **5** (0.0121 mg, 0.0230 mmol) was dissolved in CD_2Cl_2 and TMSCl (60.0 μL, 0.474 mmol) was added dropwise to the CD_2Cl_2-5 solution. $Fe(acac)_3$ (15.3 mg, 0.043 mmol) was added to the content of the NMR tube and sonicated for 15 min. The resulting solution was left to stir for 8 h and then filtered through celite. The red filtrate was concentrated down and layered with hexanes and left in a freezer at −35 C freezer overnight. Red crystals (3.8 mg, 37.1%) were collected. An aliquot gave ESI and ^{1}H NMR spectra as observed in *route 1* above (see SI, Figures S7 and S8).

*Converting from [($^{Bu}C^iC^iC^{Bu}$)$_2$Fe]Cl, **2a** or [($^{Bu}C^iC^iC^{Bu}$)$_2$Fe]I, **2b** to [($^{Bu}C^iC^iC^{Bu}$)$FeCl_2$], **4**.* In a 5 mL scintillation vial, **2a** (25.8 mg, 0.035 mmol) or **2b** (23.3 mg, 0.031 mmol) was dissolved in 3 mL of THF. The solution was cooled to 0 °C and TMSCl (90 μL, 0.63 mmol) was added dropwise. The solution was stirred until it reached room temperature. $FeCl_3$ (9.4 mg, 0.058 mmol) was added and stirred for 8 h, resulting in a brick red mixture. The mixture was filtered through celite. The filtrate was concentrated to dryness. The concentrate was dissolved in minimum DCM and then hexanes were added to precipitate out the red solid. The product was collected over frit as a red powder and then dried (11.8 mg, 41%).

■ ASSOCIATED CONTENT

Supporting Information

The Supporting Information is available free of charge at https://pubs.acs.org/doi/10.1021/acs.organomet.3c00386.

Additional experimental procedures and spectroscopic and crystallographic data (PDF)

Crystallographic data (XYZ)

Accession Codes

CCDC 2206354−2206355 contain the supplementary crystallographic data for this paper. These data can be obtained free of charge via www.ccdc.cam.ac.uk/data_request/cif, or by emailing data_request@ccdc.cam.ac.uk, or by contacting The Cambridge Crystallographic Data Centre, 12 Union Road, Cambridge CB2 1EZ, UK; fax: +44 1223 336033.

■ AUTHOR INFORMATION

Corresponding Authors

Igor V. Rubtsov − *Department of Chemistry, Tulane University, New Orleans, Louisiana 70118, United States;* orcid.org/0000-0002-3010-6207; Email: irubtsov@tulane.edu

Charles Edwin Webster − *Department of Chemistry, Mississippi State University, Mississippi, Mississippi State 39762, United States;* orcid.org/0000-0002-6917-2957; Email: ewebster@chemistry.msstate.edu

T. Keith Hollis − *Department of Chemistry, Mississippi State University, Mississippi, Mississippi State 39762, United States;* orcid.org/0000-0002-5470-9811; Email: khollis@chemistry.msstate.edu

Authors

Joshua Mensah − *Department of Chemistry, Mississippi State University, Mississippi, Mississippi State 39762, United States*

Venkata K. Adiraju − *Department of Chemistry, Mississippi State University, Mississippi, Mississippi State 39762, United States*

James D. Cope − *Department of Chemistry, Mississippi State University, Mississippi, Mississippi State 39762, United States;* orcid.org/0000-0002-0917-0730

Robert W. Lamb − *Department of Chemistry, Mississippi State University, Mississippi, Mississippi State 39762, United States*

Xiao X. Li − *Department of Chemistry, Tulane University, New Orleans, Louisiana 70118, United States*

Bruno Donnadieu − *Department of Chemistry, Mississippi State University, Mississippi, Mississippi State 39762, United States*

Complete contact information is available at: https://pubs.acs.org/10.1021/acs.organomet.3c00386

Notes

The authors declare no competing financial interest.

■ ACKNOWLEDGMENTS

We gratefully acknowledge the National Science Foundation (Grant OIA 1539035, TI 1827686, CHE-2102552 to CEW, CHE-1954854 to IVR) and Mississippi State Chemistry Department of Chemistry for the support. We acknowledge Dr. Aaron Huckaba for early work on this project. We appreciate Dr. Qiaoli Liang of the University of Alabama in Tuscaloosa for conducting the MS/MS experiment.

■ REFERENCES

(1) Pecak, J.; Stöger, B.; Mastalir, M.; Veiros, L. F.; Ferreira, L. P.; Pignitter, M.; Linert, W.; Kirchner, K. Five-Coordinate Low-Spin

{FeNO}7 PNP Pincer Complexes. *Inorg. Chem.* **2019**, *58* (7), 4641−4646.
(2) Peris, E.; Crabtree, R. H. Key Factors in Pincer Ligand Design. *Chem. Soc. Rev.* **2018**, *47* (6), 1959−1968.
(3) Bedford, R. B.; Betham, M.; Bruce, D. W.; Davis, S. A.; Frost, R. M.; Hird, M. Iron Nanoparticles in the Coupling of Alkyl Halides with Aryl Grignard Reagents. *Chem. Commun.* **2006**, *219* (13), 1398−1400.
(4) Nath Jha, B.; Singh, N. Raghuvanshi, A. Catalytic Activity of Iron N-Heterocyclic Carbene Complexes. In *Organic Synthesis*; IntechOpen, 2020; pp 1−25.
(5) Sonnenberg, J. F.; Wan, K. Y.; Sues, P. E.; Morris, R. H. Ketone Asymmetric Hydrogenation Catalyzed by P-NH-P′ Pincer Iron Catalysts: An Experimental and Computational Study. *ACS Catal.* **2017**, *7* (1), 316−326.
(6) Helgert, T. R.; Hollis, T. K.; Valente, E. J. Synthesis of Titanium CCC-NHC Pincer Complexes and Catalytic Hydroamination of Unactivated Alkenes. *Organometallics* **2012**, *31* (8), 3002−3009.
(7) McGuinness, D. S.; Gibson, V. C.; Steed, J. W. Bis(Carbene)-Pyridine Complexes of the Early to Middle Transition Metals: Survey of Ethylene Oligomerization and Polymerization Capability. *Organometallics* **2004**, *23* (26), 6288−6292.
(8) Dierks, P.; Kruse, A.; Bokareva, O. S.; Al-Marri, M. J.; Kalmbach, J.; Baltrun, M.; Neuba, A.; Schoch, R.; Hohloch, S.; Heinze, K.; Seitz, M.; Kühn, O.; Lochbrunner, S.; Bauer, M. Distinct Photodynamics of κ-N and κ-C Pseudoisomeric Iron(Ii) Complexes. *Chem. Commun.* **2021**, *57* (54), 6640−6643.
(9) Liu, Y.; Djurovich, P. I.; Haiges, R.; Thompson, M. E. Synthesis and Photophysical Characterization of a Bis-Pincer Osmium Complex. *Polyhedron* **2014**, *84*, 136−143.
(10) Gravogl, L.; Heinemann, F. W.; Munz, D.; Meyer, K. An Iron Pincer Complex in Four Oxidation States. *Inorg. Chem.* **2020**, *59* (8), 5632−5645.
(11) Nakanishi, K.; Jimenez-Halla, J. O. C.; Yamazoe, S.; Nakamoto, M.; Shang, R.; Yamamoto, Y. Synthesis and Isolation of an Anionic Bis(Dipyrido-Annulated) N-Heterocyclic Carbene CCC-Pincer Iridium(III) Complex by Facile C-H Bond Activation. *Inorg. Chem.* **2021**, *60* (13), 9970−9976.
(12) Denny, J. A.; Lamb, R. W.; Reilly, S. W.; Donnadieu, B.; Webster, C. E.; Hollis, T. K. Investigation of Metallation/Transmetallation Reactions to Synthesize a Series of CCC−NHC Co Pincer Complexes and Their X-Ray Structures. *Polyhedron* **2018**, *151*, 568−574.
(13) Pf, M. L.; Mn, M.; De Bruin, B.; Bill, E.; Bothe, E.; Weyhermu, T.; Wieghardt, K. Molecular and Electronic Structures of Bis (Pyridine-2, 6-Diimine) Metal Complexes. *Inorg. Chem.* **2000**, *39*, 2936−2947.
(14) Benson, C. R.; Hui, A. K.; Parimal, K.; Cook, B. J.; Chen, C. H.; Lord, R. L.; Flood, A. H.; Caulton, K. G. Multiplying the Electron Storage Capacity of a Bis-Tetrazine Pincer Ligand. *Dalt. Trans.* **2014**, *43* (17), 6513−6524.
(15) Billups, J. R.; Fokakis, Z. N.; Creutz, S. E. Octahedral Iron Complexes of Pyrazine(Diimine) Pincers: Ligand Electronic Effects and Protonation. *Inorg. Chem.* **2020**, *59* (20), 15228−15239.
(16) Braun, J. D.; Gray, P. A.; Sidhu, B. K.; Nemez, D. B.; Herbert, D. E. Zn-Templated Synthesis of Substituted (2,6-Diimine)Pyridine Proligands and Evaluation of Their Iron Complexes as Anolytes for Flow Battery Applications. *Dalt. Trans.* **2020**, *49* (45), 16175−16183.
(17) Park, H. J.; Kim, K. H.; Choi, S. Y.; Kim, H. M.; Lee, W. I.; Kang, Y. K.; Chung, Y. K. Unsymmetric Ru(II) Complexes with N-Heterocyclic Carbene and/or Terpyridine Ligands: Synthesis, Characterization, Ground-and Excited-State Electronic Structures and Their Application for DSSC Sensitizers. *Inorg. Chem.* **2010**, *49* (16), 7340−7352.
(18) Liu, Y.; Harlang, T.; Canton, S. E.; Chábera, P.; Suárez-Alcántara, K.; Fleckhaus, A.; Vithanage, D. A.; Göransson, E.; Corani, A.; Lomoth, R.; Sundström, V.; Wärnmark, K. Towards Longer-Lived Metal-to-Ligand Charge Transfer States of Iron(II) Complexes: An N-Heterocyclic Carbene Approach. *Chem. Commun.* **2013**, *49* (57), 6412−6414.
(19) Son, S. U.; Park, K. H.; Lee, Y. S.; Kim, B. Y.; Choi, C. H.; Lan, M. S.; Jang, Y. H.; Jang, D. J.; Chung, Y. K. Synthesis of Ru(II) Complexes of N-Heterocyclic Carbenes and Their Promising Photoluminescence Properties in Water. *Inorg. Chem.* **2004**, *43* (22), 6896−6898.
(20) Hopkinson, M. N.; Richter, C.; Schedler, M.; Glorius, F. An Overview of N-Heterocyclic Carbenes. *Nature* **2014**, *510* (7506), 485−496.
(21) Therrien, J. A.; Wolf, M. O.; Patrick, B. O. Polyannulated Bis(N-Heterocyclic Carbene)Palladium Pincer Complexes for Electrocatalytic CO2 Reduction. *Inorg. Chem.* **2015**, *54* (24), 11721−11732.
(22) Öztürk, B. Ö.; Çetinel, B.; Karabulut Şehitoğlu, S. Encapsulation of N-Heterocyclic Carbene−Gold (I) Catalysts within Magnetic Core/Shell Silica Gels: A Reusable Alkyne Hydration Catalyst. *Appl. Organomet. Chem.* **2020**, *34* (9), 1−9.
(23) Nagata, A.; Akagi, Y.; Masoud, S. S.; Yamanaka, M.; Kittaka, A.; Uesugi, M.; Odagi, M.; Nagasawa, K. Stereoselective Synthesis of Four Calcitriol Lactone Diastereomers at C23 and C25. *J. Org. Chem.* **2019**, *84* (12), 7630−7641.
(24) Herrmann, W. A.; Böhm, V. P.; Gstöttmayr, C. W.; Grosche, M.; Reisinger, C.; Weskamp, T. Synthesis, Structure and Catalytic Application of Palladium(II) Complexes Bearing N-Heterocyclic Carbenes and Phosphines. *J. Organomet. Chem.* **2001**, *617−618*, 616−628.
(25) Herrmann, W. A. N-Heterocyclic Carbenes: A New Concept in Organometallic Catalysis. *Angew. Chemie Int. Ed.* **2002**, *41* (8), 1290−1309.
(26) Gürbüz, N.; Özdemir, I.; Demir, S.; Çetinkaya, B. Improved Palladium-Catalyzed Coupling Reactions of Aryl Halides Using Saturated N-Heterocarbene Ligands. *J. Mol. Catal. A Chem.* **2004**, *209* (1−2), 23−28.
(27) Andrew, R. E.; Gonzalez-Sebastian, L.; Chaplin, A. B. NHC-Based Pincer Ligands: Carbenes with a Bite. *Dalt. Trans.* **2016**, *45* (4), 1299−1305.
(28) Riener, K.; Haslinger, S.; Raba, A.; Högerl, M. P.; Cokoja, M.; Herrmann, W. A.; Kühn, F. E. Chemistry of Iron N -Heterocyclic Carbene Complexes: Syntheses, Structures, Reactivities, and Catalytic Applications. *Chem. Rev.* **2014**, *114* (10), 5215−5272.
(29) Schwarz, J.; Böhm, V. P. W.; Gardiner, M. G.; Grosche, M.; Herrmann, W. A.; Hieringer, W.; Raudaschl-Sieber, G. Polymer-Supported Carbene Complexes of Palladium: Well-Defined, Air-Stable, Recyclable Catalysts for the Heck Reaction. *Chem. - A Eur. J.* **2000**, *6* (10), 1773−1780.
(30) Jackson, B. J.; Najera, D. C.; Matson, E. M.; Woods, T. J.; Bertke, J. A.; Fout, A. R. Synthesis and Characterization of (DIPP CCC)Fe Complexes: A Zwitterionic Metalation Method and CO 2 Reactivity. *Organometallics* **2019**, *38* (15), 2943−2952.
(31) Egorova, K. S.; Ananikov, V. P. Toxicity of Metal Compounds: Knowledge and Myths. *Organometallics* **2017**, *36* (21), 4071−4090.
(32) Hans Wedepohl, K. The Composition of the Continental Crust. *Geochim. Cosmochim. Acta* **1995**, *59* (7), 1217−1232.
(33) Fajardo, J.; Peters, J. C. Tripodal P3XFe-N2Complexes (X = B, Al, Ga): Effect of the Apical Atom on Bonding, Electronic Structure, and Catalytic N2-to-NH3Conversion. *Inorg. Chem.* **2021**, *60* (2), 1220−1227.
(34) Lancaster, K. M.; Roemelt, M.; Ettenhuber, P.; Hu, Y.; Ribbe, M. W.; Neese, F.; Bergmann, U.; DeBeer, S. X-Ray Emission Spectroscopy Evidences a Central Carbon in the Nitrogenase Iron-Molybdenum Cofactor. *Science (80-.).* **2011**, *334* (6058), 974−977.
(35) Cook, B. J.; Polezhaev, A. V.; Chen, C. H.; Pink, M.; Caulton, K. G. Deprotonation, Chloride Abstraction, and Dehydrohalogenation as Synthetic Routes to Bis-Pyrazolate Pyridyl Iron(II) Complexes. *Eur. J. Inorg. Chem.* **2017**, *2017* (34), 3999−4012.
(36) Danopoulos, A. A.; Tsoureas, N.; Wright, J. A.; Light, M. E. N-Heterocyclic Pincer Dicarbene Complexes of Iron(II): C-2 and C-5

https://doi.org/10.1021/acs.organomet.3c00386
Organometallics XXXX, XXX, XXX−XXX

Metalated Carbenes on the Same Metal Center. *Organometallics* **2004**, *23* (2), 166−168.
(37) Giannoccaro, P.; Vasapollo, G.; Nobile, C. F.; Sacco, A. 2,6-Bis(Diphenylphosphinomethyl)Pyridine Complexes of Nickel(II), Cobalt(II), Iron(II). *Inorg. Chim. Acta* **1982**, *61* (C), 69−75.
(38) Chen, F.; Liu, N.; Dai, B. Iron(II) Bis-CNN Pincer Complex-Catalyzed Cyclic Carbonate Synthesis at Room Temperature. *ACS Sustain. Chem. Eng.* **2017**, *5* (10), 9065−9075.
(39) Regenauer, N. I.; Settele, S.; Bill, E.; Wadepohl, H.; Roşca, D. A. Bis(Imino)Pyrazine-Supported Iron Complexes: Ligand-Based Redox Chemistry, Dearomatization, and Reversible C-C Bond Formation. *Inorg. Chem.* **2020**, *59* (4), 2604−2612.
(40) Glatz, M.; Holzhacker, C.; Bichler, B.; Mastalir, M.; Stöger, B.; Mereiter, K.; Weil, M.; Veiros, L. F.; Mösch-Zanetti, N. C.; Kirchner, K. Fe II Carbonyl Complexes Featuring Small to Bulky PNP Pincer Ligands − Facile Substitution of κ 2 P, N -Bound PNP Ligands by Carbon Monoxide. *Eur. J. Inorg. Chem.* **2015**, *2015* (30), 5053−5065.
(41) Ibrahim, A. D.; Tokmic, K.; Brennan, M. R.; Kim, D.; Matson, E. M.; Nilges, M. J.; Bertke, J. A.; Fout, A. R. Monoanionic Bis(Carbene) Pincer Complexes Featuring Cobalt(I-III) Oxidation States. *Dalt. Trans.* **2016**, *45* (24), 9805−9811.
(42) Danopoulos, A. A.; Wright, J. A.; Motherwell, W. B. Molecular N2 Complexes of Iron Stabilised by N-Heterocyclic 'pincer' Dicarbene Ligands. *Chem. Commun.* **2005**, *6*, 784−786.
(43) Reilly, S. W.; Webster, C. E.; Hollis, T. K.; Valle, H. U. Transmetallation from CCC-NHC Pincer Zr Complexes in the Synthesis of Air-Stable CCC-NHC Pincer Co(Iii) Complexes and Initial Hydroboration Trials. *Dalt. Trans.* **2016**, *45* (7), 2823−2828.
(44) Rummelt, S. M.; Darmon, J. M.; Yu, R. P.; Viereck, P.; Pabst, T. P.; Turner, Z. R.; Margulieux, G. W.; Gu, S.; Chirik, P. J. Synthesis, Structure, and Hydrogenolysis of Pyridine Dicarbene Iron Dialkyl Complexes. *Organometallics* **2019**, *38* (16), 3159−3168.
(45) Pony Yu, R.; Hesk, D.; Rivera, N.; Pelczer, I.; Chirik, P. J. Iron-Catalysed Tritiation of Pharmaceuticals. *Nature* **2016**, *529* (7585), 195−199.
(46) Taniguchi, W.; Ito, J.-I.; Yamashita, M. CNC-Pincer Iron Complexes Containing a Bis(N-Heterocyclic Carbene)Amido Ligand: Synthesis and Application to Catalytic Hydrogenation of Alkenes. *J. Organomet. Chem.* **2020**, *923*, No. 121436.
(47) Wile, B. M.; Trovitch, R. J.; Bart, S. C.; Tondreau, A. M.; Lobkovsky, E.; Milsmann, C.; Bill, E.; Wieghardt, K.; Chink, P. J. Reduction Chemistry of Aryl- and Alkyl-Substituted Bis(Imino)-Pyridine Iron Dihalide Compounds: Molecular and Electronic Structures of [(PDI)2Fe] Derivatives. *Inorg. Chem.* **2009**, *48* (9), 4190−4200.
(48) Huckaba, A. J.; Cao, B.; Hollis, T. K.; Valle, H. U.; Kelly, J. T.; Hammer, N. I.; Oliver, A. G.; Webster, C. E. Platinum CCC-NHC Benzimidazolyl Pincer Complexes: Synthesis, Characterization, Photostability, and Theoretical Investigation of a Blue-Green Emitter. *Dalt. Trans.* **2013**, *42* (24), 8820.
(49) Helgert, T. R.; Hollis, T. K.; Oliver, A. G.; Valle, H. U.; Wu, Y.; Webster, C. E. Synthesis, Characterization, and X-Ray Molecular Structure of Tantalum CCC-N-Heterocyclic Carbene (CCC-NHC) Pincer Complexes with Imidazole- and Triazole-Based Ligands. *Organometallics* **2014**, *33* (4), 952−958.
(50) Huckaba, A. J.; Hollis, T. K.; Howell, T. O.; Valle, H. U.; Wu, Y. Synthesis and Characterization of a 1,3-Phenylene-Bridged N-Alkyl Bis(Benzimidazole) CCC-NHC Pincer Ligand Precursor: Homo-bimetallic Silver and Rhodium Complexes and the Catalytic Hydrosilylation of Phenylacetylene. *Organometallics* **2013**, *32* (1), 63−69.
(51) Cope, J. D.; Liyanage, N. P.; Kelley, P. J.; Denny, J. A.; Valente, E. J.; Webster, C. E.; Delcamp, J. H.; Hollis, T. K. Electrocatalytic Reduction of CO2 with CCC-NHC Pincer Nickel Complexes. *Chem. Commun.* **2017**, *53* (68), 9442−9445.
(52) Rubio, R. J.; Andavan, G. T. S.; Bauer, E. B.; Hollis, T. K.; Cho, J.; Tham, F. S.; Donnadieu, B. Toward a General Method for CCC N-Heterocyclic Carbene Pincer Synthesis: Metallation and Trans-metallation Strategies for Concurrent Activation of Three C−H Bonds. *J. Organomet. Chem.* **2005**, *690* (23), 5353−5364.
(53) Najera, D. C.; Peñas-Defrutos, M. N.; García-Melchor, M.; Fout, A. R. γ-Agostic Interactions in (MesCCC)Fe-Mes(L) Complexes. *Chem. Commun.* **2022**, *58* (69), 9626−9629.
(54) Thedford Keith Hollis, C. E. W. UNSYMMETRIC CCC - NHC PINCER METAL COMPLEXES AND METHODS OF USE THEREOF. United States Pat. Appl. Publ. 2020, US 2020/00 (PCT/US18/23659).
(55) Denny, J. A.; Lang, G. M.; Hollis, T. K. CCC-NHC Pincer Complexes: Synthesis, Application and Catalysis. In *Pincer Compounds Chemistry and Application*; Morales-Morales, D., Ed.; Elsevier, 2018; pp 251−272.
(56) Evans, D. F. The Determination of the Paramagnetic Susceptibility of Substances in Solution by Nuclear Magnetic Resonance. *J. Chem. Soc.* **1959**, 2003.
(57) Darmawan, N.; Yang, C. H.; Mauro, M.; Raynal, M.; Heun, S.; Pan, J.; Buchholz, H.; Braunstein, P.; De Cola, L. Efficient Near-UV Emitters Based on Cationic Bis-Pincer Iridium(III) Carbene Complexes. *Inorg. Chem.* **2013**, *52* (19), 10756−10765.
(58) Shields, B. J.; Kudisch, B.; Scholes, G. D.; Doyle, A. G. Long-Lived Charge-Transfer States of Nickel(II) Aryl Halide Complexes Facilitate Bimolecular Photoinduced Electron Transfer. *J. Am. Chem. Soc.* **2018**, *140* (8), 3035−3039.
(59) Cope, J. D.; Sheridan, P. E.; Galloway, C. J.; Awoyemi, R. F.; Stokes, S. L.; Emerson, J. P. Synthesis and Characterization of a Tetradentate, N-Heterocyclic Carbene Copper(II) Complex and Its Use as a Chan-Evans-Lam Coupling Catalyst. *Organometallics* **2020**, *39* (24), 4457−4464.
(60) Addison, A. W.; Rao, T. N.; Reedijk, J.; van Rijn, J.; Verschoor, G. C. Synthesis, Structure, and Spectroscopic Properties of Copper-(<scp > II</Scp>) Compounds Containing Nitrogen−Sulphur Donor Ligands; the Crystal and Molecular Structure of Aqua[1,7-Bis(N-Methylbenzimidazol-2′-Yl)-2,6-Dithiaheptane]Copper(<scp > II</Scp>) Pe. *J. Chem. Soc., Dalton Trans.* **1984**, *7*, 1349−1356.
(61) Böttcher, T.; Bassil, B. S.; Zhechkov, L.; Heine, T.; Röschenthaler, G. V. (NHCMe)SiCl4: A Versatile Carbene Transfer Reagent-Synthesis from Silicochloroform. *Chem. Sci.* **2013**, *4* (1), 77−83.
(62) Silva Valverde, M. F.; Theuergarten, E.; Bannenberg, T.; Freytag, M.; Jones, P. G.; Tamm, M. Frustrated N-Heterocyclic Carbene-Silylium Ion Lewis Pairs. *Dalt. Trans.* **2015**, *44* (20), 9400−9408.
(63) Turner, Z. R.; Bellabarba, R.; Tooze, R. P.; Arnold, P. L. Addition-Elimination Reactions across the M-C Bond of Metal N-Heterocyclic Carbenes. *J. Am. Chem. Soc.* **2010**, *132* (12), 4050−4051.
(64) Brown, R. S.; Slebocka-Tilk, H.; Buschek, J. M.; Ulan, J. G. Hydrolyses of 2-Trimethylsilyl N^Heterocycles. Involvement of Zwitterions in the Hydrolysis of 2-(Trimethylsilyl)-Af-Methylimidazole, 2-(Trimethylsilyl)Pyridine, and 2-((Trimethylsilyl)Methyl)-N-Methylimidazole. *J. Am. Chem. Soc.* **1984**, *106*, 5979 DOI: 10.1021/ja00332a038.
(65) Liao, C.; Zhu, X.; Sun, X. G.; Dai, S. Investigation of Carbon-2 Substituted Imidazoles and Their Corresponding Ionic Liquids. *Tetrahedron Lett.* **2011**, *52* (41), 5308−5310.
(66) Zeitler, K. Photoredox Catalysis with Visible Light. *Angew. Chemie - Int. Ed.* **2009**, *48* (52), 9785−9789.
(67) Thompson, D. W.; Ito, A.; Meyer, T. J. [Ru(Bpy)3]2+* and Other Remarkable Metal-to-Ligand Charge Transfer (MLCT) Excited States. *Pure Appl. Chem.* **2013**, *85* (7), 1257−1305.
(68) Vougioukalakis, G. C.; Philippopoulos, A. I.; Stergiopoulos, T.; Falaras, P. Contributions to the Development of Ruthenium-Based Sensitizers for Dye-Sensitized Solar Cells. *Coord. Chem. Rev.* **2011**, *255* (21−22), 2602−2621.
(69) Creutz, C.; Chou, M.; Netzel, T. L.; Okumura, M.; Sutin, N. Lifetimes, Spectra, and Quenching of the Excited States of Polypyridine Complexes of Iron(II), Ruthenium(II), and Osmium-(II). *J. Am. Chem. Soc.* **1980**, *102* (4), 1309−1319.

https://doi.org/10.1021/acs.organomet.3c00386
Organometallics XXXX, XXX, XXX−XXX

(70) Chábera, P.; Liu, Y.; Prakash, O.; Thyrhaug, E.; Nahhas, A. El; Honarfar, A.; Essén, S.; Fredin, L. A.; Harlang, T. C. B.; Kjær, K. S.; et al. A Low-Spin Fe(III) Complex with 100-Ps Ligand-to-Metal Charge Transfer Photoluminescence. *Nature* **2017**, *543* (7647), 695−699.
(71) Liu, Y.; Kjær, K. S.; Fredin, L. A.; Chábera, P.; Harlang, T.; Canton, S. E.; Lidin, S.; Zhang, J.; Lomoth, R.; Bergquist.; et al. A Heteroleptic Ferrous Complex with Mesoionic Bis(1,2,3-Triazol-5-Ylidene) Ligands: Taming the MLCT Excited State of Iron(II). *Chem. - A Eur. J.* **2015**, *21* (9), 3628−3639.
(72) Mengel, A. K. C. C.; Förster, C.; Breivogel, A.; Mack, K.; Ochsmann, J. R.; Laquai, F.; Ksenofontov, V.; Heinze, K. A Heteroleptic Push-Pull Substituted Iron(II) Bis(Tridentate) Complex with Low-Energy Charge-Transfer States. *Chem. - A Eur. J.* **2015**, *21* (2), 704−714.
(73) Bozic-Weber, B.; Constable, E. C.; Housecroft, C. E. Light Harvesting with Earth Abundant D-Block Metals: Development of Sensitizers in Dye-Sensitized Solar Cells (DSCs). *Coord. Chem. Rev.* **2013**, *257* (21−22), 3089−3106.
(74) Liu, L.; Duchanois, T.; Etienne, T.; Monari, A.; Beley, M.; Assfeld, X.; Haacke, S.; Gros, P. C. A New Record Excited State 3 MLCT Lifetime for Metalorganic Iron(Ii) Complexes. *Phys. Chem. Chem. Phys.* **2016**, *18* (18), 12550−12556.
(75) Zimmer, P.; Burkhardt, L.; Friedrich, A.; Steube, J.; Neuba, A.; Schepper, R.; Müller, P.; Flörke, U.; Huber, M.; Lochbrunner, S.; et al. The Connection between NHC Ligand Count and Photophysical Properties in Fe(II) Photosensitizers: An Experimental Study. *Inorg. Chem.* **2018**, *57* (1), 360−373.
(76) Li, X.; Valdiviezo, J.; Banziger, S. D.; Zhang, P.; Ren, T.; Beratan, D. N.; Rubtsov, I. V. Symmetry Controlled Photo-Selection and Charge Separation in Butadiyne-Bridged Donor-Bridge-Acceptor Compounds. *Phys. Chem. Chem. Phys.* **2020**, *22* (17), 9664−9676.
(77) Vargas, V. C.; Rubio, R. J.; Keith Hollis, T.; Salcido, M. E. Organic Synthesis with Palladium Compounds. *Org. Lett.* **1995**, *100* (2), 47.
(78) Frisch, M. J.; Trucks, G. W.; Schlegel, H. B.; Scuseria, G. E.; Robb, Ma.; Cheeseman, J. R.; Scalmani, G.; Barone, V.; Petersson, G. A.; Nakatsuji, H. *Gaussian 16, Revision A. 03*; Gaussian. Inc.: Wallingford CT, 2016; Vol. *3*.
(79) Henderson, T. M.; Izmaylov, A. F.; Scalmani, G.; Scuseria, G. E. Can Short-Range Hybrids Describe Long-Range-Dependent Properties? *J. Chem. Phys.* **2009**, *131* (4), No. 044108.
(80) Weigend, F.; Ahlrichs, R. Balanced Basis Sets of Split Valence, Triple Zeta Valence and Quadruple Zeta Valence Quality for H to Rn: Design and Assessment of Accuracy. *Phys. Chem. Chem. Phys.* **2005**, *7* (18), 3297−3305.
(81) Andrienko, G. A. Chemcraft-Graphical Software for Visualization of Quantum Chemistry Computations. See https//www.chemcraftprog.com 2010. Date accessed August 11, 2023.

https://doi.org/10.1021/acs.organomet.3c00386
Organometallics XXXX, XXX, XXX−XXX